International Journal of Automotive Technology, Vol. 7, No. 5, pp. 609–618 (2006)

1229-9138/2006/029-12

LMI-BASED H_∞ LATERAL CONTROL OF AN AUTONOMUS VEHICLE BY LOOK-AHEAD SENSING

C. S. KIM[1)*], S. Y. KIM[1)], J. H. RYU[1)] and M. H. LEE[2)]

[1)]Department of Mechanical and Intelligent Systems Engineering, Pusan National University, Busan 609-735, Korea
[2)]School of Mechanical Engineering, Pusan National University, Busan 609-735, Korea

(Received 26 December 2005; Revised 25 May 2006)

ABSTRACT–This paper presents the lateral control of an autonomous vehicle by using a look-ahead sensing system. In look-ahead sensing by an absolute positioning system, a reference lane, constructed by straight lanes or circular lanes, was switched by a segment switching algorithm. To cope with sensor noise and modeling uncertainty, a robust LMI-based H_∞ lateral controller was designed by the feedback of lateral offset and yaw angle error at the vehicle look-ahead. In order to verify the safety and the performance of lateral control, a scaled-down vehicle was developed and the location of the vehicle was detected by using an ultrasonic local positioning system. In the mechatronic scaled-down vehicle, the lateral model and parameters are verified and estimated by a J-turn test. For the lane change and reference lane tracking, the lateral controllers are used experimentally. The experimental results show that the H_∞ controller is robust and has better performance compared with look-down sensing.

KEY WORDS : Autonomous vehicle, Lateral control, LMI based H_∞ control, Look-ahead sensing, Ultrasonic local positioning system, Scale-down vehicle

NOMENCLATURE

(x_p, y_p) : vehicle position in x–y plane
φ_p : heading of vehicle
v : the lateral velocity of vehicle at C.G.
u : the longitudinal velocity of vehicle at C.G.
δ : steering angle
m : the vehicle total mass
I_{ZZ} : the yaw moment of inertia
l : wheelbase of vehicle
a/b : the distance from the vehicle C.G. to the front/rear axles
a_y : the lateral acceleration of vehicle
γ : the yaw rate of vehicle
C_f/C_r : the front/rear cornering stiffnesses
L : look-ahead distance from C.G.
ρ_{ref} : curvature of the reference lane
ϕ_T : the target yaw angle
y_e : lateral offset at the look-ahead position
ϕ_e : yaw angle error
β_T : target slip angle toward the target point
d_T : target distance
$r_T(i)$: the radius of the ith circular lane
$x_0(i)$: the initial x position of the ith lane on global coordinate
$y_0(i)$: the initial y position of the ith lane on global coordinate
$\varphi_0(i)$: the starting yaw angle of the ith lane starting point
c_0/s_0 : $\cos\varphi_0$ and $\sin\varphi_0$
c_p/s_p : $\cos\varphi_0$ and $\sin\varphi_0$

*Corresponding author. e-mail: kcsup@pusan.ac.kr

1. INTRODUCTION

One of the fundamental goals of the intelligent transportation systems (ITS) community is to develop automated highways where vehicles are capable of automatically driving down the road, either individually or in platoons of multiple vehicles. In order to implement such a system, a controller that can keep the vehicle centered in the lane is required. There are many factors that make automatic lateral control of a vehicle difficult. These include changing vehicle parameters (tire pressure, tire wear, etc.) and changing road conditions (rain, ice, bumps, crowns, etc.) as well as disturbances caused by wind and other factors (Byrne *et al.*, 1998). The partners for advanced transit and highways (PATH) program has been investigating a frequency shaped linear quadratic optimal control approach for the lateral controller. Makela and Numers (2001) have navigated and controlled a vehicle to transport heavy steel slabs by a fusion of dead reckoning of radar and passive beacons to

bury RF tags. Rossetter *et al.* (2004) presented a potential fields lane keeping assistance system by using a novel combination of a multi-antenna GPS and precision read maps. In order to design a lateral control for an autonomous vehicle, Makela and Numers (2001) used P-controller, where the front wheel is steered to minimize the heading error and the rear wheels are steered to minimize the positioning error. A lateral control algorithm based on a non-slip model (Tsugawa, 1994, 1999) could not be used when vehicle side-slip occurred. Ryu *et al.* (2004) introduced a lateral controller to minimize the target slip angle and modified it by using the information of distance to target point. Most nonlinear controllers have some advantages in that they demand no linear model and have quick response (Ackermann *et al.*, 1995; Sampei *et al.*, 1995), but they have inadequate robustness against severely varying disturbances and modeling uncertainties. In this paper, LMI-based H_∞ control by feedback from lateral offset and yaw angle error is used to design a robust lateral controller against the high frequency sensor noise and modeling uncertainty.

The remainder of this paper is organized as follows. Section 2 provides the construction of a reference lane, the calculation skill of lane information and the state space vehicle model. The algorithm for lane switching, conventional lateral control and LMI-based H_∞ control are described. Section 3 explains the configuration of the ultrasonic local positioning system and the scaled-down vehicle. In section 4, the designed lateral controllers are simulated and tested. Section 5 summarizes the results presented in this paper.

2. LATERAL CONTROL BY LOOK-AHEAD SENSING

2.1. Lateral Vehicle Models

In a previous research (Tsugawa, 1994; 1999), the dynamics of a vehicle is described as follows:

$$\dot{x}_p = v\cos\varphi,$$
$$\dot{y}_p = v\sin\varphi, \text{ and} \tag{1}$$
$$\dot{\varphi}_p = \frac{v}{l}\tan\delta.$$

These relations hold when the vehicle drives without slip. However, in the case of an actual vehicle, the tire slip cannot be ignored. So, yaw rate and lateral acceleration as lateral performance are calculated by the classical single-track model which is obtained by lumping the two front wheels as one wheel in the centerline of the vehicle, and doing the same with the two rear wheels (Choi *et al.*, 2002). Tires can be modeled as linear within $|a_y| \le 0.3g$. For the state $X=[v\ \gamma\ \varphi_p]^T$ and δ, the state space of a vehicle is described as

$$\begin{bmatrix}\dot{v}\\ \dot{\gamma}\\ \dot{\varphi}_p\end{bmatrix} = \begin{bmatrix}a_{11} & a_{12} & 0\\ a_{21} & a_{22} & 0\\ 0 & 1 & 0\end{bmatrix}\begin{bmatrix}v\\ \gamma\\ \varphi_p\end{bmatrix} + \begin{bmatrix}b_1\\ b_2\\ 0\end{bmatrix}\delta, \tag{2}$$

where

$a_{11}=-2(C_f+C_r)/mu$, $a_{12}=-u-2(aC_f-bC_r)/mu$,

$a_{21}=-2(aC_f-bC_r)/I_{zz}u$, $a_{22}=-2(a^2C_f+b^2C_r)/I_{zz}u$,

$b_1=2C_f/m$, $b_2=2aC_f/I_{zz}$.

Due to the motion of the vehicle and the change of road geometry, the equations capturing the evolution of y_e and φ_e at L are given by

$$\dot{y}_e = u\cdot\varphi_e - v - L\cdot\gamma, \tag{3}$$

$$\dot{\varphi}_e = u\cdot\rho_{ref} - \gamma. \tag{4}$$

By the combination of the 2 d.o.f. vehicle dynamics and the sensor dynamics, a state space equation for the state vector $X_0=[v\ \gamma\ \varphi_e\ y_e]^T$ and the output vector $Y_0=[\varphi_e\ y_e]^T$ is written as

$$\dot{X}_0 = A_0X_0 + B_{01}\rho_{ref} + B_{02}u, \tag{5}$$
$$Y_0 = C_0X_0$$

where $A_0=\begin{bmatrix}a_{11} & a_{12} & 0 & 0\\ a_{21} & a_{22} & 0 & 0\\ 0 & -1 & 0 & 0\\ -1 & -L & u & 0\end{bmatrix}$,

$B_{01}=\begin{bmatrix}0\\0\\u\\0\end{bmatrix}$, $B_{02}=\begin{bmatrix}b_1\\b_2\\0\\0\end{bmatrix}$ and $C_0=\begin{bmatrix}0 & 0 & 1 & 0\\ 0 & 0 & 0 & 1\end{bmatrix}$.

2.2. Reference Lane Look-ahead Information

Reference lanes are constructed simply by the combination of straight lanes or circular lanes. One segment of a lane is represented by

$$\text{Ref}_i=\{r_T(i),\ x_0(i),\ y_0(i),\ \varphi_0(i)\}. \tag{6}$$

In contrast with a mobile robot, a vehicle cannot always pass over the reference lane, owing to side slip and steer-

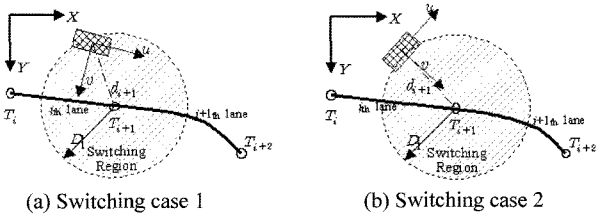

(a) Switching case 1 (b) Switching case 2

Figure 1. The segment switching in the reference lane.

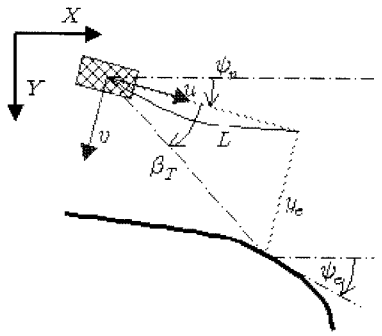

Figure 2. Look-ahead information of lane.

ing limitation. Thus, the ith segment of the reference lane is switched to the next i+1th segment, when the distance, d_{i+1}, between the next starting point, T_{i+1}, and the current point, (x_p, y_p), is smaller than D_1 as shown in Figure 1. (a). The other case of switching is fulfilled when the distance, d_{i+1}, is increased relative to the previous one, which prevents a vehicle from diverging as shown in Figure 1 (b). As a result, the segment is switched either

$$d_{i+1} \le D_1 \text{ or } [d_{i+1}]_k \ge [d_{i+1}]_{k-1} + D_2, \tag{7}$$

where the subscript k is the time sequence and D_2 is a constant.

Figure 2 shows the reference lane information for the given L, where β_T is obtained as

$$\beta_T = \tan^{-1}\left(\frac{y_e}{L}\right). \tag{8}$$

In an absolute positioning system such as a global or local positioning system, (x_p, y_p) and φ_p can be measured directly. To find y_e from the sensed position and the known reference lane, the reference lane in the fixed coordinate should be transformed to the one in the body coordinate. For the straight reference lane ($\varphi_T = \varphi_0$), the lateral offset and the yaw angle error can be derived as

$$y_e = \frac{(s_0 c_p - c_0 s_p)L + [s_0(x_p - x_0) - c_0(y_p - y_0)]}{s_0 s_p + c_0 c_p}, \tag{9}$$

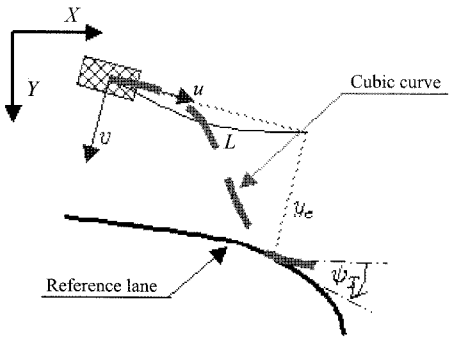

Figure 3. Trajectory generation by a cubic curve.

$$\varphi_e = \varphi_0 - \varphi_p. \tag{10}$$

For the circular lane, the lateral offset and yaw angle error can be described as

$$y_e = y_c' - \text{sign}(y_c')\sqrt{r_T^2 - (L - x_c')^2}, \tag{11}$$

$$\varphi_e = \tan^{-1}\left(\frac{L - x_c'}{y_c' - y_e}\right). \tag{12}$$

Finally, the target distance is described by

$$d_T = \sqrt{(L - x_p)^2 + (y_e - y_p)^2}. \tag{13}$$

2.3. Lateral Control of an Autonomous Vehicle

In a previous research (Tsugawa, 1994, 1999), the headings at the origin and the target point are assumed to be tangential angles of a curve going through the origin and the target point at these points. Then, a cubic curve that goes through the two points as shown in Figure 3 is uniquely defined as follows

$$y = A_t x^3 + B_t x^2, \tag{14}$$

where

$$A_t = (L \cdot \tan\varphi_T - 2y_e)/L^3, \quad B_t = (3y_e - L \cdot \tan\varphi_T)/L^2.$$

Since the desired trajectories to the target point are independent of the longitudinal velocity u in a non-slip vehicle model, the steering control angle that leads the vehicle to hit the target point (L, y_e) with the heading φ_T is given as follows

$$\delta = \tan^{-1}(2lB_t). \tag{15}$$

When the lane information is satisfied with

$$y_e(3y_e - L \cdot \tan\varphi_e) < 0. \tag{16}$$

In the research of Ryu *et al.* (2004), the basic algorithm for lateral control is to minimize β_T. Generally, the diminishment of d_T needs a greater steering angle. Considering the additive steering input by inverse proportion to d_T, the error for a controller is modified as follows

$$e = \left(K_1 + \frac{K_2}{d_T}\right)\beta_T, \tag{17}$$

where K_1 and K_2 are the gains for β_T and d_T. Finally, the lateral controller is designed by a PI controller for the modified error.

Even though the H_∞ control problem has an analytic solution in terms of Riccati equations, the LMI approach remains valuable for several reasons. First, it is applicable to all plants without restrictions on infinite or pure imaginary invariant zeros. Second, it offers a simple and insightful derivation of the Riccati-based solvability conditions. Third, it is practical thanks to availability of efficient convex optimization algorithms. The set of H_∞ controllers with closed-loop performance γ can be

implicitly parameterized by the solution (R,S) of a system of linear matrix inequalities (Gahinet and Apkarian, 1993). The matrices R and S play a role analogous to tha of Riccati solutions, X_∞ and Y_∞ in classical Riccati-based H_∞ control. In this paper, LMI-based H_∞ control is introduced to design a robust lateral controller against high frequency sensor noise and modeling uncertainty. Since the closed-loop control systems using look-ahead information are more stable than systems using look-down information, the H_∞ control is designed to regulate the lateral offset and to minimize the yaw angle error at the look-ahead distance, L. As stated in section 2.2, the information of the reference lane at the look-ahead can be calculated from absolute positioning system and reference lane. The advantage of using weighted performance specifications is obvious in multi-variable system design (Zhou and Doyle, 1998). First, some components of a vector signal are usually more important than others. Second, each component of the signal may not be measured in the same units. Therefore, weighting functions are essential to make these components comparable. For rejecting errors in a certain frequency range, some frequency-dependent weights must be chosen. The selection of weighting functions for a specific design problem often involves ad hoc fixing, much iteration, and fine tuning. It is very hard to give a general formula for weighting functions that will work in every case. Based on time domain performance specifications, the corresponding requirements in the frequency domain, in terms of the bandwidth ω_b and the peak sensitivity M_s, can be determined. A possible choice of W_e can be obtained by modifying the weighting function as follows (Zhou and Doyle, 1998).

$$W_e=\frac{s/M_s+\omega_b}{s+\omega_b\varepsilon}. \tag{18}$$

The magnitude of $|KS|$ in the low-frequency range is essentially limited by the allowable cost of control effort and the saturation limit of the actuators; hence, in general, the maximum gain M_u of KS can be fairly large, while the high-frequency gain is essentially limited by the controller bandwidth (ω_{bc}) and the sensor noise frequencies. A candidate weight W_u would be

$$W_u=\frac{s+\omega_{bc}/M_u}{\varepsilon_1 s+\omega_{bc}}, \tag{19}$$

for a small $\varepsilon_1>0$. The weighting for MIMO problems can be initially chosen as diagonal matrices, with each diagonal term chosen as above. As previously satisfied with the design specification for H_∞ controllers, the generalized plant is constructed as shown in figure 4. $G_0(s)$ is the nominal model, including the 2 d.o.f. vehicle dynamics and the sensor. $W_u(s)$ and $W_e(s)$ are the weighting functions for the input and the output of $G_0(s)$,

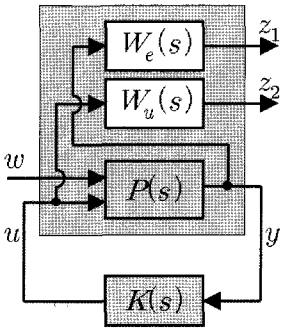

Figure 4. Generalized plant in H_∞ control.

respectively. $K(s)$ is the designed H_∞ controller. The reference input is defined as the external input ω The control objectives z_1 and z_2 represent the regulation error and the control input u. The realizations for $G_0(s)$, $W_e(s)$ and $W_u(s)$ are given by

$$G_0(s)=\begin{bmatrix}A_0 & B_0\\ C_0 & D_0\end{bmatrix},\ W_e(s)=\begin{bmatrix}A_e & B_e\\ C_e & D_e\end{bmatrix}$$

$$\text{and } W_u(s)=\begin{bmatrix}A_u & B_u\\ C_u & D_u\end{bmatrix} \tag{20}$$

Then the generalized plant can be represented as a state space model:

$$\dot{X}=\begin{bmatrix}A_e & 0 & B_eC_0\\ 0 & A_u & 0\\ 0 & 0 & A_0\end{bmatrix}X+\begin{bmatrix}0\\ 0\\ B_{01}\end{bmatrix}\rho_{ref}+\begin{bmatrix}0\\ B_u\\ B_{02}\end{bmatrix}u$$

$$Z=\begin{bmatrix}C_e & 0 & D_eC_0\\ 0 & C_u & 0\end{bmatrix}X+\begin{bmatrix}0\\ 0\end{bmatrix}\rho_{ref}+\begin{bmatrix}0\\ D_u\end{bmatrix}u \tag{21}$$

$$Y=\begin{bmatrix}0 & 0 & C_0\end{bmatrix}X\quad+[0]\rho_{ref}+[0]u$$

3. ULTRASONIC LOCAL POSITIONING SYSTEM AND A SCALED-DOWN VEHICLE

3.1. Configuration of a Scaled-down Vehicle

Figure 5 shows a 1/10 scaled-down vehicle, the wheel base and mass of which are 0.24 m and 2.105 kg. 2 wheel drive, 2 wheel steering is adopted. The maximum speed of the vehicle is 1.2 m/s. The maximum steering angle is 30°. The specification of the scaled-down vehicle, except speed, is reasonable to alter a real vehicle such as a sedan or a small-size jeep. For the positioning of the scaled-down vehicle, the ULPS is used. The information about yaw angle and TOFs is sent to a remote-control system by a wireless communication system with RS-232. The remote-control system judges the position (x_p, y_p, φ_p) and re-transmits the driving and steering commands to a CPU

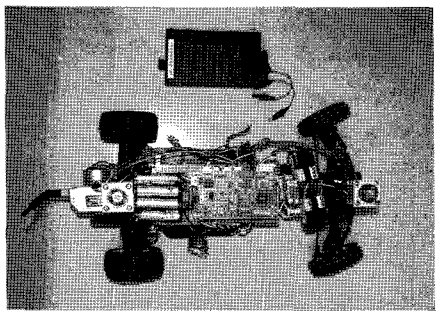

Figure 5. A scaled-down vehicle.

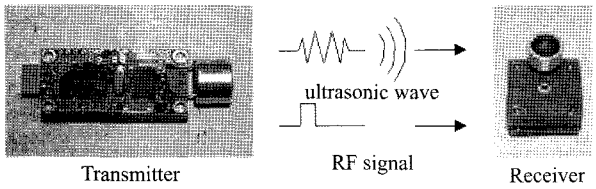

Figure 6. Configuration of ultrasonic distance measuring system.

attached to the scaled-down.

40 kHz ultrasonic transmitter with roughly 3 kHz of bandwidth is used. Considering the directive angles of the transmitter and the receiver, if transmitters are attached at 45°, the recognizing region is defined. The procedure for positioning by the ULPS is as follows. After sending ultrasonic wave and RF signals synchronously in the fixed transmitting-part as a pseudo-satellite, the receiving-part attached to a movable object acquires them. The distance information is then resent to a remote-control. Finally, the position is determined by the remote-control. Figure 6 shows the transmitting and the receiving part of the developed ULPS and the remote-control unit.

3.2. Positioning Algorithm

In this paper, a period-detecting technique is used to find the time of flight of ultrasonic waves. Comparing the results of the threshold-detecting technique (Webster, 1994; Wehn and Belanger, 1997), the proposed technique has no problem with measuring distances under 30 m. The ULPS, similar to the GPS, locates the position by using the elapsed time of waves from a indoor transmitter.

In ideal cases, the receiver position is a point of contact of the spheres with radii $d_i (i=1,\ldots, n)$ from the transmitters. So, the vector representation of an ultrasonic receiver position, $\vec{P}$, is written as

$$\left|\vec{P}-\vec{T}_i\right|=d_i, \tag{22}$$

where $\vec{T}_i=(a_i, b_i, c_i)$ are the position vectors of ultrasonic transmitters. Basically, a position can be determined by four distances from different transmitters T_1, T_2, T_3, and T_4 as follows:

$$\vec{P}\cdot(\vec{T}_1-\vec{T}_2)=D_1,\ \vec{P}\cdot(\vec{T}_2-\vec{T}_3)=D_2,\ \vec{P}\cdot(\vec{T}_3-\vec{T}_4)=D_3,$$

$$\vec{P}\cdot(\vec{T}_4-\vec{T}_1)=D_4, \tag{23}$$

where

$$D_1=\left\{\left|\vec{T}_1\right|-\left|\vec{T}_2\right|-(d_1^2-d_2^2)\right\}/2,\ D_2=\left\{\left|\vec{T}_2\right|-\left|\vec{T}_3\right|-(d_2^2-d_3^2)\right\}/2$$

$$D_3=\left\{\left|\vec{T}_3\right|-\left|\vec{T}_4\right|-(d_4^2-d_5^2)\right\}/2,\ \text{and}\ D_4=\left\{\left|\vec{T}_4\right|-\left|\vec{T}_1\right|-(d_4^2-d_1^2)\right\}/2.$$

Then the position, $P=[x_p\ y_p\ z_p]^T$, is obtained as

$$P=A^{-1}B, \tag{24}$$

where

$$A=\begin{bmatrix} a_1-a_2 & b_1-b_2 & c_1-c_2 \\ a_2-a_3 & b_2-b_3 & c_2-c_3 \\ a_3-a_4 & b_3-b_4 & c_3-c_4 \end{bmatrix}\ \text{and}\ B=\begin{bmatrix} D_1 & D_2 & D_3 & D_4 \end{bmatrix}^T.$$

Thus, the transmitters should be located in order that the inverse matrix of A in Equation (24) may exist, that is, $\det A \neq 0$. The least-square estimator is used for the errors which are linearly related to geometry.

In the positioning experimentations of the ULPS, four transmitters are fixed on the edge of the ceiling. The experiments are carried out in an indoor space of 7 m long, 4 m wide and 4 m high, under normal temperature without certain frequency noise. For the known grid points, the maximum, mean, and STD of the positioning error are 0.3384 m, 0.1830 m, and 0.0728 m, respectively. By using least-square estimation, the maximum, mean, and STD of error are reduced to 0.0172 m, 0.0095 m, and 0.0042 m, respectively. Figure 7 shows the measured and the estimated grid points. Next, to verify the positioning accuracy with respect to the moving objects, the receiver is tied to the arm of a turntable that rotates with constant angular velocities. The angles measured by the ULPS are compared with the gyro compass. Considering the velocity of a scaled-down vehicle or indoor mobile robots, the angular velocities of a turntable are 0.12, 0.20, 0.28, 0.36, and 0.44 rad/s. The results for moving points are summarized in table 1.

3.3. Vehicle Parameter Estimation and Verification

Parameters such as mass, m, distance from C.G. to the front and the rear axle, a and b, can be measured easily. However, it is difficult to measure the front and rear cornering stiffness, C_f and C_r, and the yaw moment of inertia, I_{zz}. The unknown parameters can be estimated by the least-square algorithm as mentioned in the previous

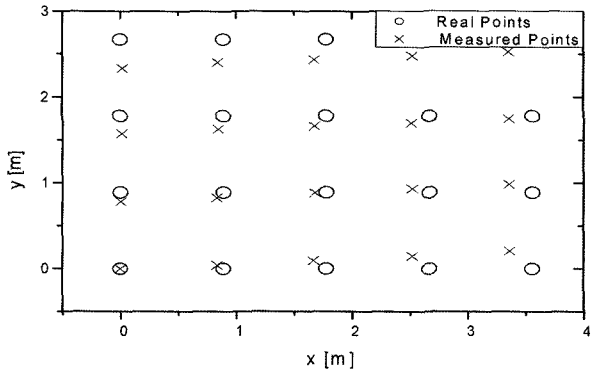

(a) Measured points

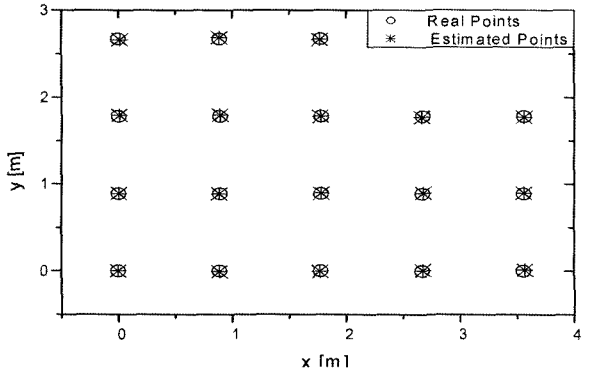

(b) Estimated points by LSE

Figure 7. Least-square estimation of the grid points.

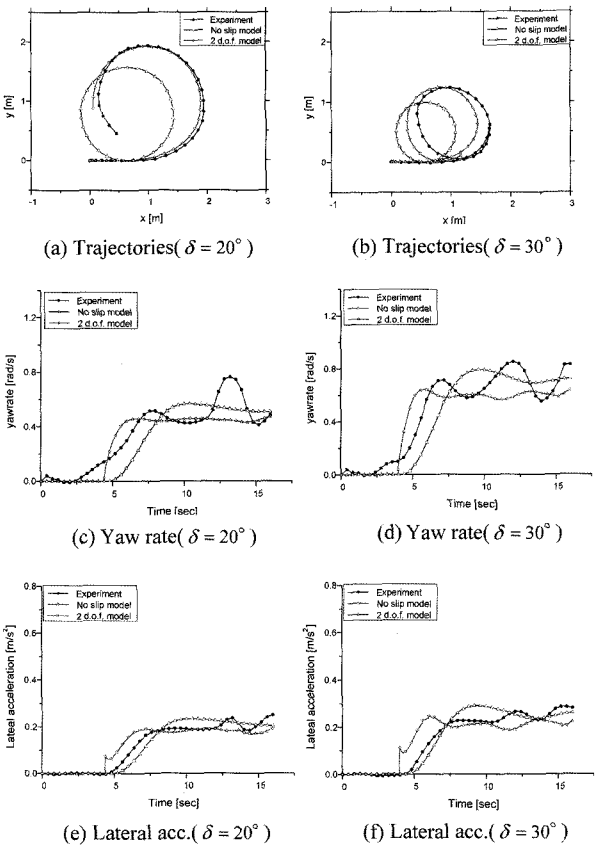

(a) Trajectories($\delta = 20°$)
(b) Trajectories($\delta = 30°$)
(c) Yaw rate($\delta = 20°$)
(d) Yaw rate($\delta = 30°$)
(e) Lateral acc.($\delta = 20°$)
(f) Lateral acc.($\delta = 30°$)

Figure 8. Parameter estimation results under u=0.5 m/s.

section. For the parameter estimation, Equation (2) is reconstructed as follows

$$(2v+2a\gamma-2u\delta)\cdot C_f+(2v-2b\gamma)\cdot C_r=-(muv+mu^2\gamma),$$
$$u\dot{\gamma}\cdot I_{zz}+(2av+2a^2\gamma-2au\delta)\cdot C_f+(2b^2\gamma-2bv)\cdot C_r=0 \quad (25)$$

where the output is acquired by a J-turn test with 0.5 m/s velocity and 0.3491 rad (20°) steering angle. Figure 8 shows the results of parameter estimation, where the vehicle position is sensed by the ULPS. The main factor causing the mismatch in the results may be due to the nonlinearity of the tires, the limitation of wheel alignment, or the steering delay.

4. EXPERIMENTATION FOR THE LATERAL CONTROL

The lateral controllers were then experimented for the lane change and the reference lane tracking. Considering the highway width (3.5 m) and the vehicle tread (2.5 m), the settling time in the scaled-down system is set up when the C.G. of vehicle is settled within 0.05 m. The look-ahead distance is set at 0.6 m and the segment switching

Table 1. Positioning results of moving points.

Angular velocity [rad/s]	Positioning errors [m]			Angle errors [rad]					
				ULPS			Gyro compass		
	Mean	Max.	STD	Mean	Max.	STD	Mean	Max.	STD
0.12	0.038	0.135	0.017	−0.024	−0.389	0.040	−0.009	−0.185	0.076
0.20	0.051	0.096	0.019	−0.045	−0.205	0.035	−0.046	−0.206	0.073
0.28	0.083	0.193	0.025	−0.086	−0.426	0.051	−0.084	−0.222	0.064
0.36	0.121	0.185	0.026	−0.133	−0.281	0.035	−0.153	−0.274	0.057
0.44	0.130	0.183	0.028	−0.141	−0.233	0.039	−0.188	−0.333	0.062

Table 2. Lane change results in simulation.

Control Type	Vel. [m/s]	Lateral responses		Steering input [rad]		Yaw rate [rad/s]		Lateral acceleration [m/s^2]	
		overshoot [m]	setling time [s]	max.	STD	max.	STD	max.	STD
Tsugawa	0.35	−0.101	5.6	0.541	0.147	0.613	0.152	0.234	0.038
	0.50	−0.549	–	–	–	–	–	–	–
	0.70	−0.600	–	–	–	–	–	–	–
Target slip angle	0.35	−0.035	3.6	0.541	0.099	0.551	0.100	0.234	0.028
	0.50	−0.126	7.6	0.541	0.138	0.619	0.165	0.292	0.048
	0.70	−0.268	18.8	0.541	0.226	0.862	0.327	0.370	0.087
H_∞ control	0.35	−0.049	3.6	0.541	0.086	0.521	0.083	0.234	0.033
	0.50	−0.122	6.4	0.541	0.107	0.589	0.121	0.292	0.049
	0.70	−0.218	8.8	0.541	0.140	0.635	0.180	0.370	0.076

distance, D_1, is 0.3 m. At the corner of ULPS sensing range, positioning errors are abruptly increased. To remove the errors, a 2nd-order Butterworth lowpass filter is applied in spite of time delay. The lateral control of Tsugawa failed in experimentation because of positioning error in the ULPS. Simulations were performed to compare to each performance of controller by Matlab tool box, and results were listed in Table 2 and 3.

4.1. Lane Change Results

In the lane change maneuvering, the scale-down vehicle started with 0.35 m lateral offset and 0 rad yaw angle error. Table 2 shows lane change simulation results. LMI-based H_∞ controller and target slip angle controller show similar responses as shown in Figure 9 and 10. On the other hand, as the vehicle velocity increases, the target slip angle controller fails to carry out a lane change. Comparing with the target slip angle control, the H_∞ controller has similar overshoot, but the settling time of the H_∞ controller is smaller.

4.2. Lane Tracking Results

For reference lane tracking, a reference lane is given as shown in Figure 11. The length of straight lane is 2 m and the radius is selected as 1.3 m in order to reflect the limitation of indoor driving space and the side slip under low velocity.

The lateral control of Tsugawa cannot track the reference lane either. As shown in Figure 12, lateral control by target slip angle cannot achieve lane tracking as the

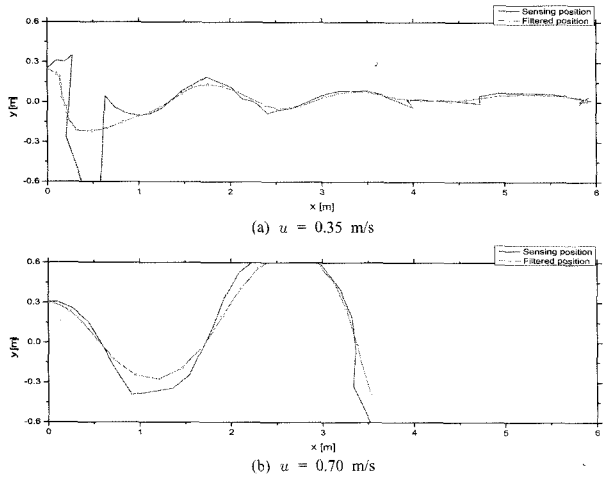

(a) u = 0.35 m/s

(b) u = 0.70 m/s

Figure 9. Trajectories in lane change experimentations by target slip angle control.

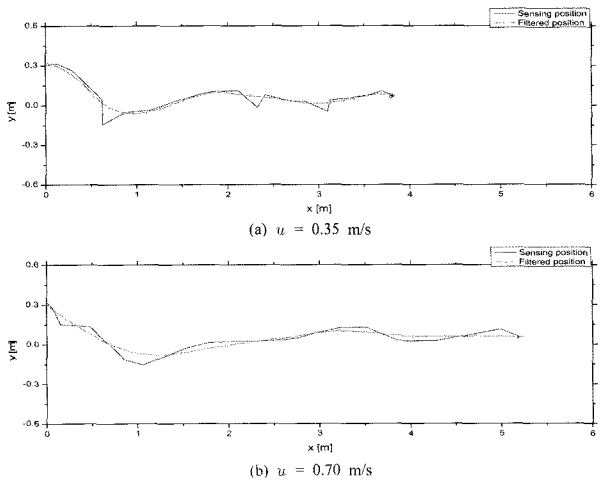

(a) u = 0.35 m/s

(b) u = 0.70 m/s

Figure 10. Trajectories in lane change experimentations by H_∞ control.

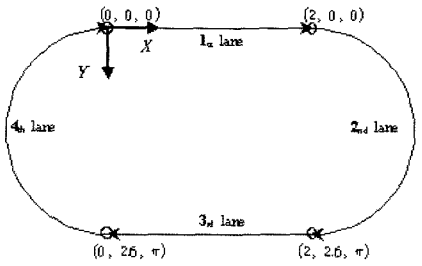

Figure 11. Reference lane for tracking.

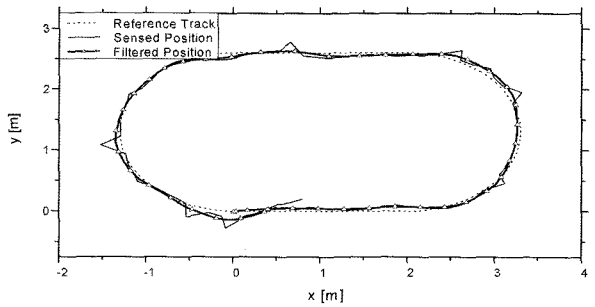

(a) $u = 0.35m/s$

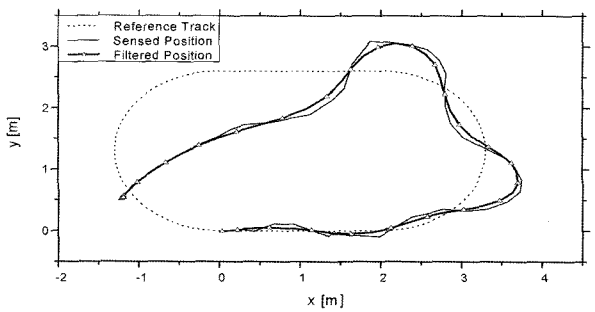

(b) $u = 0.70m/s$

Figure 12. Trajectories in lane tracking experimentations by target slip angle control.

vehicle velocity increase. At high vehicle velocity, the vehicle controlled by target slip angle error breaks away from the lane but an H_∞ lateral controller enables it to track the lane as shown in Figure 13.

The look-ahead distance, L, is important in the lateral control by using a look-ahead sensing system. To compare look-ahead sensing (L=0.6, 1.0 m) with look-down sensing (L=0.2 m), lane tracking by H_∞ control is performed under the different look-ahead distances.

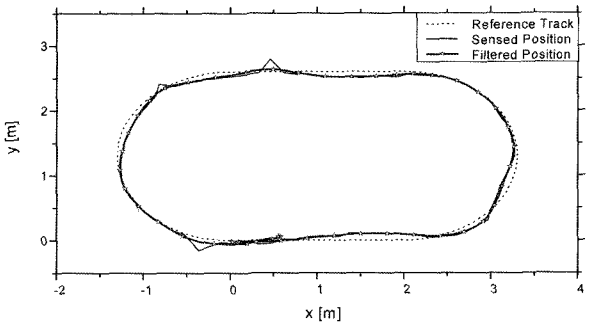

(a) $u = 0.35m/s$

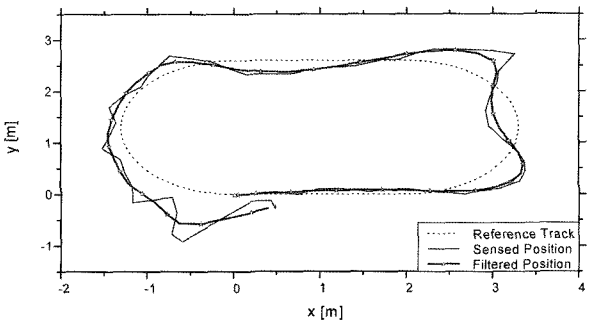

(b) $u = 0.70m/s$

Figure 13. Trajectories in lane tracking experimentat-ions by H_∞ control.

Table 3. Lane tracking responses in simulation.

Control type	Velocity [m/s]	Steering input [rad]		Yaw rate [rad/s]		Lateral acceleration [m/s^2]	
		max.	STD	max.	STD	max.	STD
Tsugawa	0.35	0.351	0.134	0.390	0.148	0.122	0.046
	0.50	0.541	0.201	0.748	0.273	0.239	0.095
	0.70	–	–	–	–	–	–
Target slip angle	0.35	0.267	0.115	0.300	0.127	0.100	0.042
	0.50	0.422	0.159	0.590	0.222	0.221	0.084
	0.70	–	–	–	–	–	–
H_∞ control	0.35	0.325	0.121	0.285	0.126	0.152	0.052
	0.50	0.541	0.148	0.494	0.202	0.292	0.087
	0.70	0.541	0.223	0.986	0.343	0.429	0.140

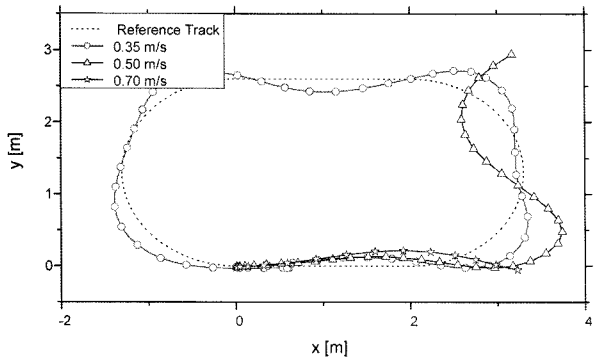

(a) $L = 0.20m$

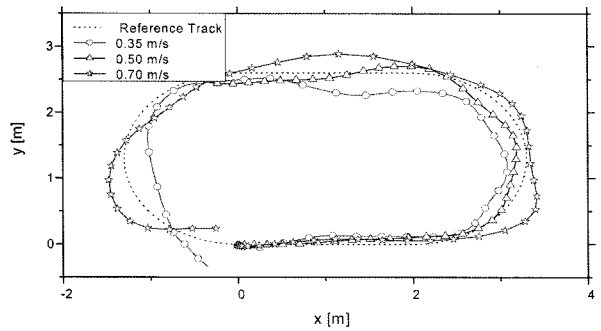

(b) $L = 1.00m$

Figure 14. Trajectories of each look-ahead distance (H_∞ control).

Since common look-down sensors have been attached on the front bumper, the case of L=0.2 m comes under look-down sensing. In Figure 14 (a), look-down sensing cannot cope with the rapid change of lane curvature. Table 3 shows lane tracking simulation results.

5. CONCLUSION

This paper presented the lateral control of an autonomous vehicle by using a look-ahead sensing system. In look-ahead sensing by an absolute positioning system, a reference lane was simply constructed by a combination of straight and circular lanes. To switch from a segment of lane to the next segment, a segment switching algorithm was introduced. To cope with sensor noise and modeling uncertainty, a robust LMI-based H_∞ lateral controller was designed by the feedback of lateral offset and yaw angle error at the look-ahead of the vehicle. Conventional lateral control algorithms using look-ahead sensing were described.

To verify the performance of the lateral control, a scaled-down vehicle was developed, where the location of the vehicle was detected using the ULPS. In the 2 d.o.f. lateral model of the scaled-down vehicle, cornering stiffness and moment of inertia were estimated by least-square estimation. The lateral controllers by Tsugawa, target slip angle, and H_∞ control were simulated and tested for lane change and reference lane tracking. In lane change maneuvering, the controller by Tsugawa failed in lane change when velocity increased. The designed H_∞ controller had a smaller settling time and STD of steering input, but the lateral acceleration was similar to conventional controls. In the lane tracking maneuvering at high velocity, the vehicle controlled by Tsugawa's method and target slip angle broke away from the lane, but the H_∞ controller was robust against modeling uncertainty. In the experimentation, Tsugawa's lateral control could not track the reference lane, but H_∞ lateral controller was able to do so. Compared with look-down sensing, the H_∞ lateral control by the look-ahead information had better performance.

REFERENCES

Ackermann, J., Guldner, J., Sienel, W., Steinhauser, R., and Utkin, V. I. (1995). Linear and nonliner controller design for robust automatic steering. *IEEE Trans. Control Systems Technology* **3, 1,** 132–143.

Byrne, R. H., Abdallah, C. T. and Dorato, P. (1998). Experimental results in robust lateral control of highway vehicles. *IEEE Control Systems Magazine* **18, 2,** 70–76.

Choi, J. Y., Hong, S. J., Park, K. T., Yoo, W. S. and Lee, M. H. (2002). Lateral control of autonomous vehicle by yaw rate feedback. *J. Mechanical Science and Technology* **16, 3,** 338–343.

Gahinet, P. and Apkarian, P. (1993). An LMI-based parameterization of all H_∞ controllers with applications. *Proc. IEEE Conf. Decision and Control,* 656–661.

Makela, H. and Numers, T. V. (2001). Development of a navigation and control system for an autonomous outdoor vehicle in a steel plant. *Control Engineering Practice,* **9,** 573–583.

Rossetter, E. J., Switkes, J. P. and Gerdes, J. C. (2004). Experimental validation of the potential field lane-keeping system. *Int. J. Automotive Technology* **5, 5,** 95–108.

Ryu, J. H., Chang, Y. S., Park, G. H., Lee, C. H., Park, S. H. and Lee, M. H. (2004). Research on Navigation System of an Autonomous Vehicle Using RTK-DGPS. *The 30th Annual Conf. IEEE Industrial Electronics Society,* **2,** 1716–1720.

Sampei, M., Tamura, T., Kobayashi, T. and Shibui, N. (1995). Arbitrary path tracking control of articulated vehicles using nonliner control theory. *IEEE Trans. Control Systems Technology* **3, 1,** 125–131.

Tsugawa, S. (1994). Vision-based vehicles in Japan: machine vision systems and driving control systems. *IEEE Trans. Industrial Electronics* **41, 4,** 389–405.

Tsugawa, S. (1999). An overview on control algorithms for automated highway systems. *IEEE/IEEJ/JSAI Int. Conf.*, 234–239.

Webster, D. (1994). A pulsed ultrasonic distance measurement system based upon phase digitizing. *IEEE Trans. Instrumentation and Measurement* **43, 4,** 578–582.

Wehn, H. W. and Belanger, P. R. (1997). Ultrasound-based robot position estimation. *IEEE Trans. Robotics and Automation* **13, 5,** 682–692.

Zhou, K. and Doyle, J. C. (1998). *Essentials of Robust Control.* Prentice-Hall Int.